The dynamic Atg13-free conformation of the Atg1 EAT domain is required for phagophore expansion

Mary G. Lin[a], Johannes Schöneberg[a], Christopher W. Davies[a,†], Xuefeng Ren[a], and James H. Hurley[a,b,*]

[a]Department of Molecular and Cell Biology and California Institute for Quantitative Biosciences, University of California, Berkeley, Berkeley, CA 94720; [b]Molecular Biophysics and Integrated Bioimaging Division, Lawrence Berkeley National Laboratory, Berkeley, CA 94720

ABSTRACT **Yeast macroautophagy begins with the de novo formation of a double-membrane phagophore at the preautophagosomal structure/phagophore assembly site (PAS), followed by its expansion into the autophagosome responsible for cargo engulfment. The kinase Atg1 is recruited to the PAS by Atg13 through interactions between the EAT domain of the former and the tMIM motif of the latter. Mass-spectrometry data have shown that, in the absence of Atg13, the EAT domain structure is strikingly dynamic, but the function of this Atg13-free dynamic state has been unclear. We used structure-based mutational analysis and quantitative and superresolution microscopy to show that Atg1 is present on autophagic puncta at, on average, twice the stoichiometry of Atg13. Moreover, Atg1 colocalizes with the expanding autophagosome in a manner dependent on Atg8 but not Atg13. We used isothermal titration calorimetry and crystal structure information to design an EAT domain mutant allele *ATG1^{DD}* that selectively perturbs the function of the Atg13-free state. Atg1^{DD} shows reduced PAS formation and does not support phagophore expansion, showing that the EAT domain has an essential function that is separate from its Atg13-dependent role in autophagy initiation.**

Monitoring Editor
Suresh Subramani
University of California, San Diego

Received: Apr 24, 2017
Revised: Mar 6, 2018
Accepted: Mar 9, 2018

INTRODUCTION

Autophagy is an essential process in cells whereby destruction of cellular components supports cellular renewal, homeostasis, and survival under stresses ranging from starvation to infection (Mizushima *et al.*, 2008; Mizushima and Komatsu, 2011). Autophagic cargoes, either bulk cytoplasmic contents or selectively targeted proteins and organelles, are engulfed in a growing double-membraned structure known as the phagophore. The phagophore matures and closes to form the autophagosome, whose contents are degraded upon fusion of the autophagosome with the vacuole or lysosome (Mizushima, 2007). Autophagy occurs in all eukaryotes, and many components of the autophagic machinery are conserved among yeast, animals, and plants (Nakatogawa *et al.*, 2009; Bento *et al.*, 2016; Wen and Klionsky, 2016). Since the identification of components of the autophagic machinery beginning in yeast in the late 1990s, autophagy proteins have been broadly classified into functional clusters (Suzuki *et al.*, 2007; Mizushima *et al.*, 2011; Reggiori and Klionsky, 2013). In yeast, initiation occurs through the Atg1 complex (Papinski and Kraft, 2016), which consists of the Atg1 protein kinase and the Atg13, Atg17, Atg29, and Atg31 regulatory and scaffolding subunits. Phagophore nucleation involves the phosphatidylinositol class III complex I, the Atg18-Atg2 complex, and transmembrane protein Atg9-containing vesicles (Wen and Klionsky, 2016; Hurley and Young, 2017). This set of early steps in autophagosome biogenesis occurs at a punctate structure referred to as the PAS (preautophagosomal structure/phagophore assembly

This article was published online ahead of print in MBoC in Press (http://www.molbiolcell.org/cgi/doi/10.1091/mbc.E17-04-0258) on March 22, 2018.

†Present address: Genentech, 1 DNA Way, South San Francisco, CA 94080.

*Address correspondence to: James H. Hurley (jimhurley@berkeley.edu).

Abbreviations used: AIM, Atg8-interacting motif; DID, 1,1′ dioctadecyl-3,3,3′,3′-tetramethylindodicarbocyanine; EAT, early autophagy targeting and tethering; EGFP, enhanced green fluorescent protein; FWHM, full-width half-maximum; GST, glutathione *S*-transferase; IDR, intrinsically disordered region; ITC, isothermal titration calorimetry; LIR, LC3-interacting motif; MBP, maltose-binding protein; PAS, preautophagosomal structure/phagophore assembly site; SIM, structured illumination microscopy; YPD, yeast extract–peptone–dextrose.

© 2018 Lin *et al.* This article is distributed by The American Society for Cell Biology under license from the author(s). Two months after publication it is available to the public under an Attribution–Noncommercial–Share Alike 3.0 Unported Creative Commons License (http://creativecommons.org/licenses/by-nc-sa/3.0).

"ASCB®," "The American Society for Cell Biology®," and "Molecular Biology of the Cell®" are registered trademarks of The American Society for Cell Biology.

site). The subsequent expansion of the phagophore and recruitment of cargo rely on the conjugation of the ubiquitin-like protein Atg8 to phosphatidylethanolamine. Atg8 conjugation is carried out by the Atg12-5-16 ligase complex (Klionsky and Schulman, 2014). It commences at the PAS, but then continues throughout autophagosome expansion. In yeast, autophagosome expansion depends on Atg8, and the size of yeast autophagosomes is correlated with the availability of Atg8 (Xie *et al.*, 2008). One of the essential roles of Atg1 in autophagy initiation is the phosphorylation of Atg9, which leads to recruitment of Atg18 and triggers the lipidation of Atg8 (Papinski *et al.*, 2014). The Atg1 complex also has essential noncatalytic roles in autophagy initiation, which could include tethering and scaffolding of vesicles at the PAS (Lin and Hurley, 2016; Hurley and Young, 2017).

The Atg1 complex initiates autophagy in response to starvation and inhibition of the master growth regulator mTOR. Under growth conditions, mTOR phosphorylates Atg13; upon starvation and inhibition of mTOR, dephosphorylation of Atg13 stabilizes the assembly of the pentameric Atg1 complex (Kamada *et al.*, 2010). Atg13 directly interacts with both Atg1 and Atg17, bridging the two subcomplexes (Kabeya *et al.*, 2005; Yamamoto *et al.*, 2016). The pentameric complex forms higher-order structures by tetramerizing (Köfinger *et al.*, 2015) and by forming a meshwork through multiple Atg13-binding sites on Atg17 (Yamamoto *et al.*, 2016). Reports based on biochemical interaction differ as to whether Atg1 and Atg13 are constitutively associated regardless of cellular nutritional status, or whether they associate only under starvation conditions (Kraft *et al.*, 2012; Fujioka *et al.*, 2014). Imaging of artificially enlarged autophagosomes in Ape1-overexpressing cells showed that Atg1 and Atg13 have distinct localization patterns, with Atg1 and Atg13 both found at the PAS, but Atg1 present alone on the growing phagophore (Suzuki *et al.*, 2013). It has been shown in yeast that expression of an Atg13 mutant that cannot bind Atg1 only partially reduces autophagy (Kraft *et al.*, 2012). Similarly, mammalian cells expressing an ATG13 variant that cannot bind ULK1 in an ATG13 knockout background still show some autophagic activity (Kraft *et al.*, 2012; Hieke *et al.*, 2015). Because so much emphasis has been placed on Atg13 as the major activator of Atg1, the nature of the putative Atg13-independent functions of Atg1 is important to clarify and could have important implications for understanding the regulation of Atg1 and how it contributes to autophagosome biogenesis.

Atg1 domain structure is conserved from yeast through mammalian ULK1, with an N-terminal protein kinase domain, a central intrinsically disordered region (IDR) linker that includes phosphorylation sites and an Atg8-interacting motif (AIM; known as an LC3-interacting motif [LIR] in mammals) (Kraft *et al.*, 2012), and C-terminal tandem microtubule-interacting and transport domains (Yan *et al.*, 1998) that are collectively referred to as the EAT (early autophagy targeting and tethering) domain (Ragusa *et al.*, 2012). The EAT domain is best known as the locus of Atg13 binding (Cheong *et al.*, 2005; Kamada *et al.*, 2010; Yeh *et al.*, 2011). The EAT domain binds to the dihelical "tMIM" motif in the C-terminal IDR of Atg13 (Fujioka *et al.*, 2014). The EAT domain is also capable of tethering high-curvature vesicles through its C-terminal domain (Ragusa *et al.*, 2012). Atg9-containing vesicles have been observed at the phagophore assembly site and may serve to nucleate the formation of the phagophore (Mari *et al.*, 2010; Yamamoto *et al.*, 2012), and the idea that Atg1 could be involved in organizing vesicles at the PAS is appealing. However, tethering is observed with the isolated EAT domain, and the stoichiometric complex with Atg13 does not possess this activity (Ragusa *et al.*, 2012). Consistent with its different properties in the presence and absence of Atg13, the EAT domain has very different dynamic characteristics under these two conditions. Using hydrogen-deuterium exchange coupled to mass spectrometry, it has been shown that the EAT domain alone is highly dynamic, yet upon binding of Atg13, the EAT domain is rigidified into a normal folded domain (Stjepanovic *et al.*, 2014). Many autophagy proteins consist of a mixture of ordered and disordered regions (Popelka *et al.*, 2014; Mei *et al.*, 2016). Some of the disordered regions can become ordered upon ligation; however, this does not necessarily mean that they function only in their ordered state. The question of whether disordered states of autophagy proteins are merely inactive or latent versions of their ordered forms, or whether they have functions of their own, has been a difficult one to address. The main goal of this study was to probe whether the dynamic, Atg13-free form of Atg1 exists in vivo and whether it has a physiological role in vesicle tethering or other functions.

Atg13 consists of an N-terminal Hop1, Rev7, Mad2 fold domain that mediates downstream Atg14 recruitment (Jao *et al.*, 2013) followed by a much larger (residues 269–738) intrinsically disordered region. This region includes mTOR phosphorylation sites, the binding site for Atg1 (residues 460–521, MIM motif) (Fujioka *et al.*, 2014; Stjepanovic *et al.*, 2014), and two binding sites for Atg17 (Yamamoto *et al.*, 2016). Isothermal titration calorimetry (ITC) results show that Atg1-EAT and dephosphorylated Atg13-tMIM have a high affinity for each other, on the order of ~100 nM (Stjepanovic *et al.*, 2014). The sequences involved are reasonably well conserved in human ULK1 and ATG13. The Atg1-Atg13 subcomplex in turn associates with Atg17-Atg29-Atg31 with a lower affinity (Fujioka *et al.*, 2014; Stjepanovic *et al.*, 2014), although avidity effects presumably increase the effective affinity (Yamamoto *et al.*, 2016). Clearly, Atg13-tMIM binding is a central role for Atg1-EAT, yet the evidence described earlier for a possible Atg13-independent function of Atg1, and a report of an ATG13-independent role for the human ULK1 EAT domain (Chan *et al.*, 2009), led us to probe more deeply.

Here, we used a combination of live-cell imaging and structurally driven biochemistry to show that the Atg1 EAT domain has an essential function late in autophagosome biogenesis that is independent of Atg13. Using tracking and computational analysis of a population of cells over time and imaging of live cells with structured-illumination microscopy, we show that, under physiological conditions, Atg1 colocalizes with Atg13 only at the PAS. While Atg13 is confined to the PAS, Atg1 colocalizes around the entire autophagosomal ring; we show that Atg1 localization to the expanding autophagosome is dependent only on the AIM motif. On the basis of the Atg1-EAT:Atg13 tMIM crystal structure (Fujioka *et al.*, 2014), we engineered a mutant Atg1 EAT variant Atg1^{DD} that has normal Atg13 binding and stability but severely compromised autophagic activity. This confirms a functional role for the dynamic Atg13-free form of the EAT domain.

RESULTS

Distinct localization of Atg1 and Atg13 on the expanding phagophore

We imaged growing autophagosomes in yeast strains expressing either Atg1 or Atg13 tagged with enhanced green fluorescent protein (Atg1-3×EGFP or Atg13-3×EGFP) together with mCherry-Atg8 (Figures 1, A–E, and 2, A and B). The Atg1 and Atg13 signals reached their peak intensity (Figure 1, A and D) at the same time as Atg8, which was set as the reference time zero. The full-width half-maximum (FWHM) of the Atg1 signal grew together with the Atg8 signal over the subsequent 300 s (Figure 1B), increasing from ~250 to 400 nm. By comparison, the FHWM of the Atg13 signal remained

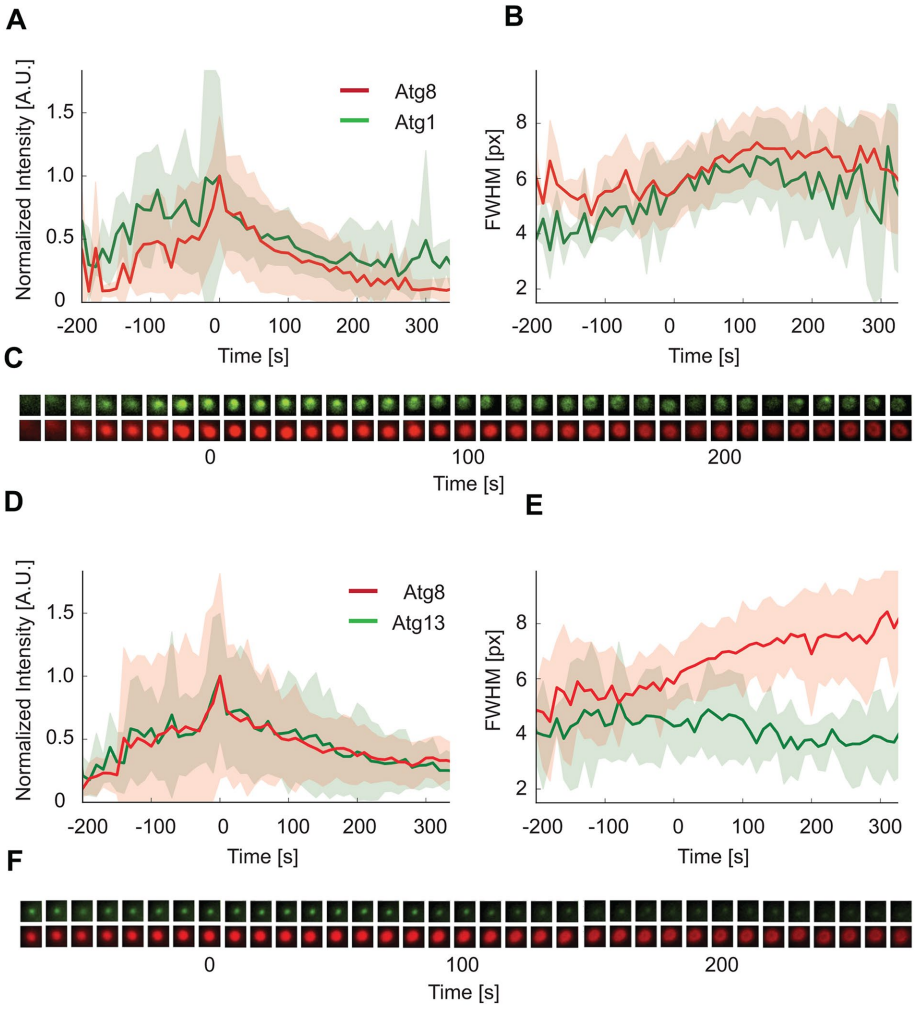

FIGURE 1: Kinetic analysis of Atg8, Atg13, and Atg1. (A) Normalized intensity of Atg8 (red) and Atg1 (green) over time shows Atg1 peaks ~20 s before Atg8. (B) FWHM fit shows that Atg1 puncta show the same widening behavior as Atg8 after peak intensity, in contrast to Atg13, which stays punctate. Solid lines: mean; shaded area: SD; $n = 27$ traces. (C) Representative fluorescence trace showing one puncta. (D) Normalized intensity of Atg8 (red) and Atg13 (green) over time shows both proteins peak at the same time in PAS formation. (E) FWHM (i.e., puncta width) fit of the puncta shows that both Atg8 and Atg13 are punctate before their intensity peak (time < 0 frames). While Atg13 stays punctate, the Atg8 punctae start to widen and eventually form rings. Solid lines: mean; shaded area: SD; $n = 38$ traces. (F) Representative fluorescence trace showing one puncta.

steady at ~250 nm over the ensuing 300 s (Figure 1E). This analysis is based on conventional diffraction-limited microscopy. Thus, the structures of apparent 250 nm size correspond to diffraction-limited puncta and thus to the PAS. The apparent ~400 nm structures were inferred (and subsequently verified below) to correspond to completed autophagosomes. These data are consistent with previous observations (Suzuki *et al.*, 2013) and suggested to us that the population of Atg1 on the expanding autophagosomes is not bound to Atg13.

We used structured illumination microscopy (SIM) to obtain high spatial resolution images of yeast cells chromosomally expressing the combinations Atg1-3×EGFP and mCherry-Atg8, and Atg13-3×EGFP and mCherry-Atg8. These strains show normal autophagy activity, as shown by mCherry-Atg8 processing (Figure 3, A and B). Autophagy was induced with rapamycin. As autophagy initiates asynchronously, we observed a mixture of initiating phagophores and complete autophagosomes. We selected complete Atg8 rings for comparative analysis. Atg13 showed a punctate localization adjacent to the ring (Figure 3A). In contrast, Atg1 was present as a ring and completely colocalized with Atg8 (Figure 3A). This is consistent with results from the bulk analysis.

Wide-field quantitative imaging to determine stoichiometry of autophagy proteins has been a useful tool for understanding the composition of the PAS (Geng *et al.*, 2008). We verified that Atg1 is more abundant than other proteins in the Atg1 complex, Atg13 and Atg17), as previously shown (Köfinger *et al.*, 2015). These measurements encompassed all observed puncta and thus represent an average over puncta corresponding to the PAS and to autophagosomes. To control for the possibility that the excess Atg1 might reflect a separate pool involved in the Atg11-dependent constitutive Cvt pathway (Yorimitsu and Klionsky, 2005), we repeated the analysis in an *atg11*Δ strain (Figure 3C). The loss of Atg11 made no difference to the stoichiometry. Thus, three lines of evidence from time-resolved imaging, superresolution imaging, and molecule counting lead to the same conclusion that there is a separate pool of Atg1 involved in phagophore expansion that is independent of Atg13.

Engineering an Atg1 variant to probe Atg13-independent function

Atg13 itself (Funakoshi *et al.*, 1997) and Atg1 binding to Atg13 (Fujioka *et al.*, 2014) are both important for initiation of the autophagosome; thus, simply deleting *ATG13*, or even just crippling the Atg13-binding site on Atg1, is not a suitable approach for fine-grained mapping of Atg13-binding independent functions of Atg1. Any effort to identify other functions of Atg1, such as lipid binding, must decouple the roles of Atg1 in lipid binding and Atg13 binding. Previously, it was shown that yeast Atg13 knockouts rescued with an Atg13 mutant unable to bind Atg1 still showed partial autophagy activity (Kraft *et al.*, 2012). We took the reciprocal approach of engineering a variant with intact Atg13 binding but intended to impair other putative functions. Our initial hypothesis was that high-curvature vesicle binding might be another function of the EAT domain (Ragusa *et al.*, 2012). Because Atg13 binding inhibits vesicle binding (Ragusa *et al.*, 2012), we reasoned that these binding sites must overlap. A series of surface-exposed hydrophobic residues protrude from the EAT domain helices involved in Atg13 binding. We reasoned that, in the dynamic Atg13-free conformation of EAT, these residues could bind to liposomes and mediate vesicle tethering. We sought to minimize the impact on Atg13 binding by mutating residues peripheral to the Atg13-binding site as defined in the *Kluyveromyces marxianus* cocrystal structure (Protein Data Bank ID: 4P1N) (Fujioka *et al.*, 2014) (Figure 4A).

The hydrophobic residues Leu-666, Met-676, Met-760, and Met-811 were mutated in the context of the *Kluyveromyces lactis* Atg1

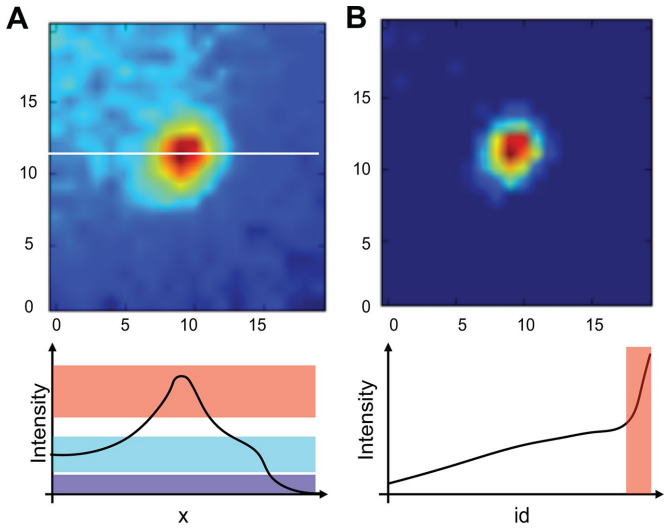

FIGURE 2: Image processing. (A) Representative PAS puncta with its intensity in the *x* dimension (white line) plotted on the bottom. Note that there are three layers of signal convoluted in the image. Dark blue: imaging background; light blue: cell background; red: PAS signal. (B) The PAS structure after removal of both imaging and cell backgrounds by taking the derivative of the image intensity and retaining only those pixels in the high slope area (red bar, bottom of puncta image).

EAT domain, which we have established as a well-behaved biochemical system (Stjepanovic *et al.*, 2014). These residues are highly conserved in the crystallized *K. marxianus*, in which they correspond to Leu-671, Met-681, Met-765, and Met-816 (Fujioka *et al.*, 2014) (Figure 4A). Targeted residues were changed to Asp in four pairwise combinations in order to maximally disrupt the putative lipid-binding function. To screen interactions quantitatively and avoid even minor perturbations in Atg13 binding, we screened mutants using ITC. Three of the double mutants, L666D/M676D, L666D/M760D, and M676/M760D, decreased affinity by a factor of four to six compared with the wild-type K_d of 100 nM (Figure 4B). These were discarded from further consideration. M760D/M811D (referred to henceforward as Atg1^{DD}), however, bound to Atg13 with a K_d of 150 nM (Figure 4B), essentially wild-type affinity. Atg1^{DD} also showed equivalent binding of glutathione *S*-transferase (GST)-Atg13 compared with wild-type Atg1 in an immunoprecipitation experiment (Figure 5A). As an additional control, we found that Atg1^{DD} also showed equivalent binding of GST-Atg8 compared with wild-type Atg1 (Figure 5B). We judged this variant to be an appropriate tool to probe for putative Atg13-independent functions.

Atg1^{DD} is defective in phagophore expansion

We constructed the *Saccharomyces cerevisiae* version of Atg1^{DD} by incorporating the mutants L809D and I874D that correspond to positions 760 and 881 of *K. lactis*, identified as described earlier. We applied the Pho8Δ60 assay to determine whether Atg1^{DD} was defective in nitrogen starvation–induced autophagy. This assay measures the vacuolar transport of a phosphatase whose normal vacuolar transport signal has been crippled, leaving it dependent on autophagy induction for its transport (Klionsky, 2007). Atg1^{DD} has negligible starvation-induced autophagic activity, comparable to that of *atg1*Δ cells transformed with an empty vector, and also shows defective mCherry-Atg8 processing (Figure 6, A and B). The Atg1^{DD} protein is expressed at the same level as wild type, however (Figure 6C). We had initially hypothesized that this mutation would lead to impaired vesicle tethering. However, the ability of the Atg1^{DD} mutant to tether lipids in vitro was unaltered (Figure 7). Many exposed hydrophobic residues remain at adjacent positions of the EAT domain helices, and it appears that these residues must be sufficient to maintain lipid tethering. It is

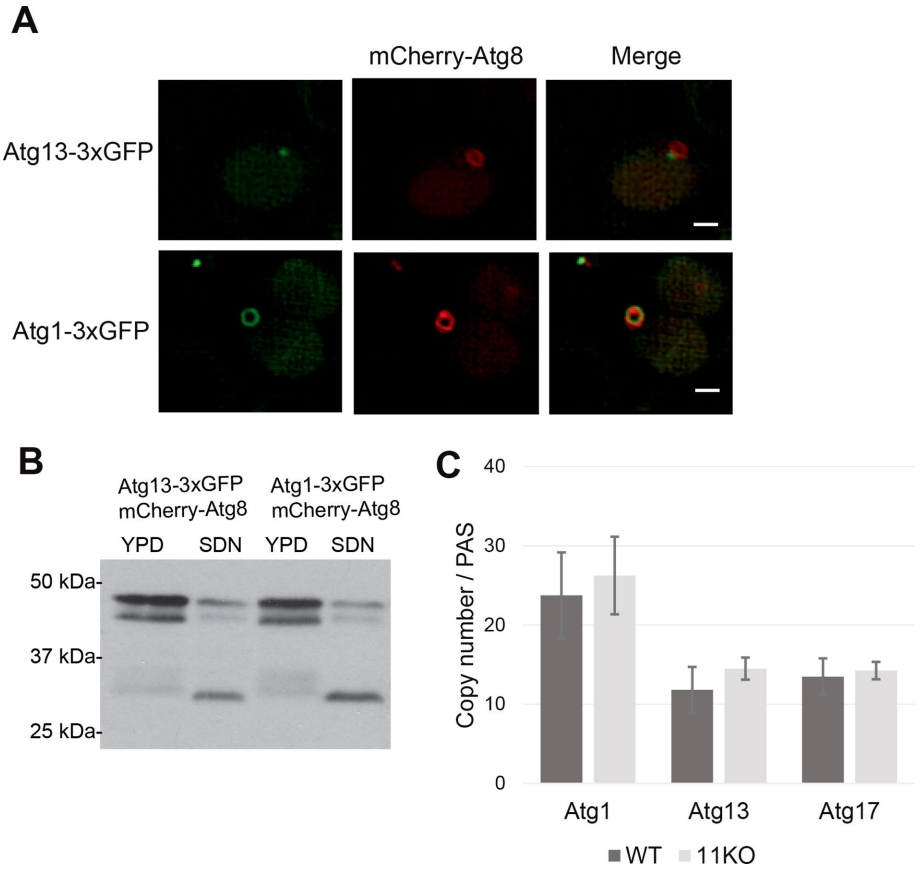

FIGURE 3: SIM and quantitative microscopy of Atg13 and Atg1. (A) SIM of Atg13 or Atg1 (3× GFP, green) or Atg8 (mCherry, red) shows that Atg1 colocalizes with Atg8 at the mature autophagosome, while Atg13 remains punctate. Scale bar: 1 μm. (B) mCherry-Atg8 processing assay of tagged strains endogenously expressing GFP-tagged Atg1 or Atg13 and mCherry-tagged Atg8. Cells were grown to log phase in rich media (YPD), and autophagy was induced by nitrogen starvation (SDN). mCherry (conjugated: 43 kDa; free: 29 kDa) was detected by Western blot. (C) Estimated copy number of autophagy proteins determined by quantitative microscopy using strain JBY404, which expresses dimeric LacO-binding protein LacI-GFP binding to 128 *LacO* repeats, as a standard (Brickner *et al.*, 2004; Köfinger *et al.*, 2015; Teis *et al.*, 2008). Values are based on integrated intensity of the puncta and are an average of three independent experiments. Error bars: SD.

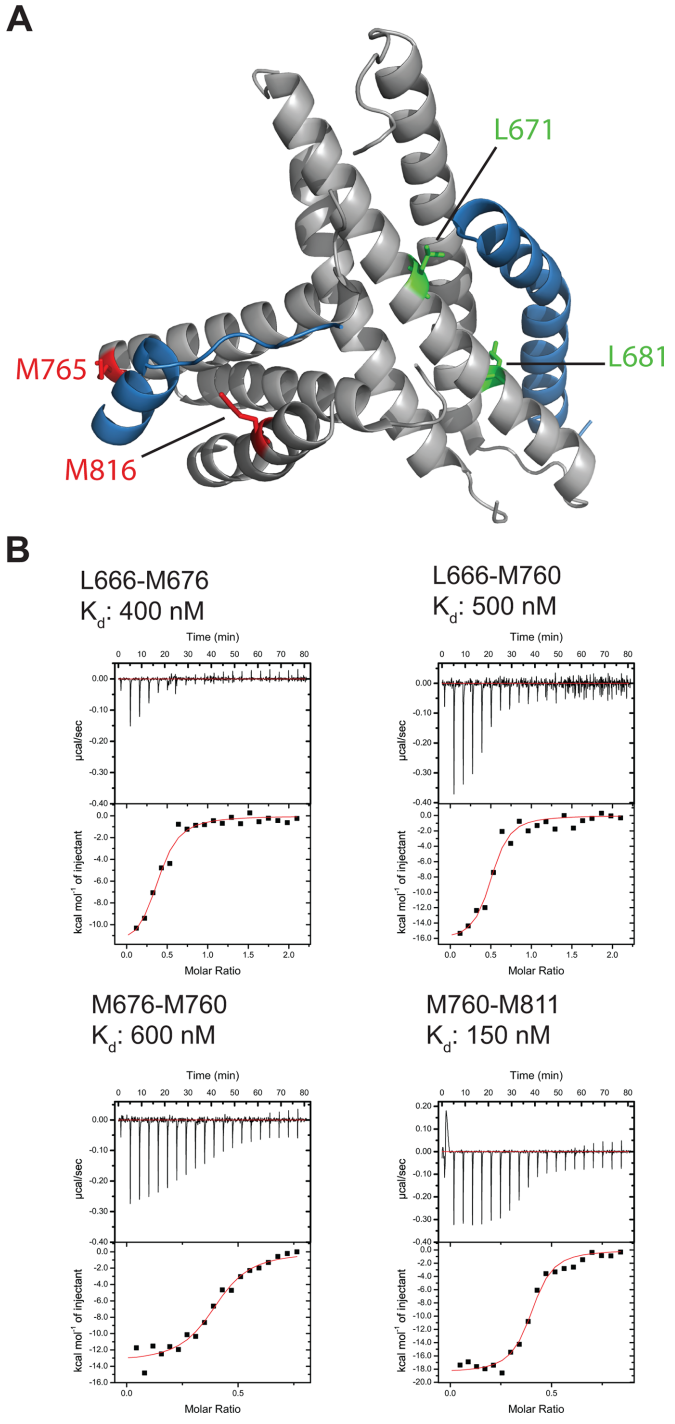

FIGURE 4: Identification of Atg1 double-aspartate mutant that binds Atg13 with wild-type affinity. (A) Structure of *K. marxianus* Atg1 EAT domain and Atg13 interaction showing mutated residues. Atg1 EAT domain: gray; Atg13: blue; mutants that decreased binding to Atg13 (L671, M681): green; mutants that retained wild-type binding to Atg13 (M765, M816): red. (B) Representative ITC thermograms showing binding affinity of Atg1 mutants with Atg13.

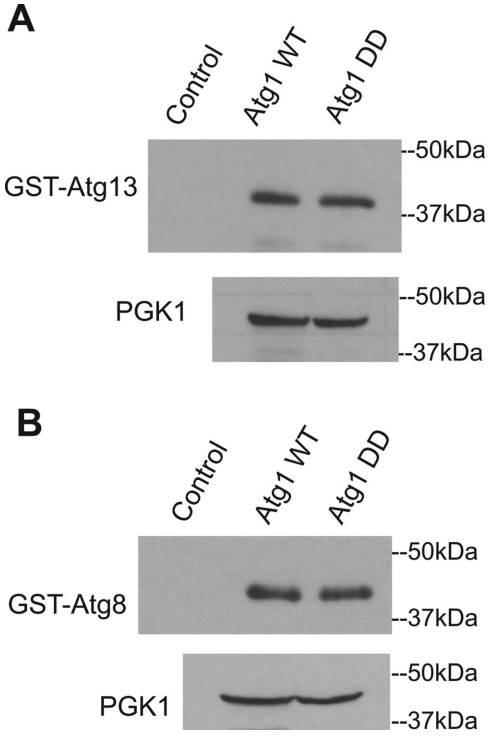

FIGURE 5: Interaction of Atg1 and Atg1^{DD} with Atg13 and Atg8. (A) Interaction between Atg1-3 × GFP and Atg1^{DD}-3 × GFP purified from cell lysate and recombinant GST-Atg13$_{432–520}$. (B) Interaction between Atg1-3 × GFP and Atg1^{DD}-3 × GFP purified from cell lysate and recombinant GST-Atg8. PGK1 is shown as a loading control. WT, wild type.

possible that the lipid-binding domain and the Atg13-binding domain of Atg1 overlap so extensively that it is not possible to decouple them mutationally. Despite the fact that the Atg1^{DD} mutant data do not resolve whether vesicle tethering is a physiological function of the EAT domain, the mutation does demonstrate that an EAT domain mutant with normal stability and full Atg13 binding is still by some means able to cripple autophagic activity.

For examining whether the Atg1^{DD} autophagy defect was linked to a change to its recruitment and localization in vivo, an *atg1Δ:ATG1^{DD}-3×EGFP mCherry-ATG8* yeast strain was generated. The strain was imaged using SIM after 1 h rapamycin treatment to induce autophagy. Only punctate Atg1- and Atg8-labeled structures were observed, reflecting that phagophores did not grow beyond the PAS stage (Figure 6D). Moreover, only ~15% of cells showed puncta formation as compared with ~30% for wild type, indicative of a decrease in recruitment even to the PAS (Figure 6D). To investigate the possibility that Atg1^{DD} was defective in localization to the growing phagophore, we restored autophagy progression by rescuing the mutant with unlabeled, wild-type Atg1 expressed on a yeast centromeric plasmid. In the rescued cells, mature Atg8-labeled ring structures were abundantly observed. Atg1^{DD} was observed on the rings and colocalized with Atg8 on essentially all of the rings seen (Figure 6D). These data show that *ATG1^{DD}* is not dominant negative and that the defect in autophagy is not due to an inability to localize to the growing phagophore.

Given that Atg1^{DD} does not interfere with localization to the growing phagophore and that Atg13 is not present, we used SIM to follow up on the previous proposal that the AIM motif of Atg1 is important for autophagosomal localization (Kraft *et al.*, 2012; Papinski and Kraft, 2016). Mutant Atg1 with substitutions V432A and E433A (Atg1^{VE}) cannot bind Atg8 (Kraft *et al.*, 2012). Moreover, it has previously been shown that Atg1^{VE} shows a strong autophagy defect in vivo, although it is still recruited to the PAS (Kraft *et al.*, 2012). Indeed, Atg1 is recruited to the PAS upstream and

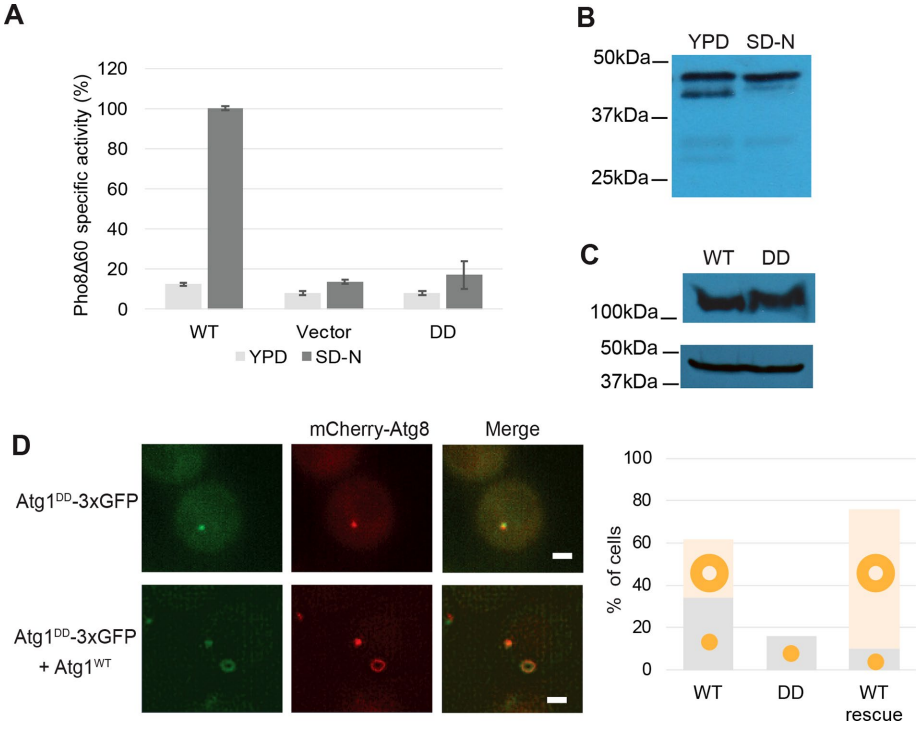

FIGURE 6: Atg1-DD shows severe autophagy defect. (A) Pho8Δ60 assay monitoring bulk autophagy was carried out in rich media (YPD) or nitrogen-starvation (SD-N) conditions. Samples were normalized to the activity of cells rescued with wild type under autophagy-inducing conditions. Results are average of three independent experiments. Error bars: SD. (B) mCherry-Atg8 processing assay showing autophagy defect in Atg1^{DD} mutant. Atg1^{DD} cells endogenously expressing mCherry-Atg8 were grown to log phase in rich media (YPD) and autophagy was induced by nitrogen starvation (SD-N). WT, wild type. mCherry (conjugated: 43 kDa; free: 29 kDa) was detected by Western blot. (C) Western blot showing expression of wild-type and double-aspartate mutant Atg1. Loading control: PGK1. (D) SIM of endogenous Atg1-DD mutant and mutant rescued with wild-type Atg1. Quantitation of distribution of structures found in mutant and rescue cell lines. Quantitation of wild-type and rescue strains was done via SIM; quantitation of the DD mutant was done in wide-field microscopy after confirming the existence of only punctate structures via structured illumination. Wild type $n = 98$; rescue $n = 52$; DD mutant $n = 168$. Scale bar: 1 μm.

independent of Atg8 (Suzuki *et al.*, 2007). We then asked whether Atg1 localization to the mature autophagosome is mediated by interaction with Atg8. We imaged *atg1Δ:ATG1^{VE}-3 × GFP mCherry-ATG8* cells and found that, consistent with the severe in vivo autophagy defect, no mature autophagosomes were observed (Figure 8, A and B). To observe the effect of the VE substitution on Atg1 localization at the ring, we again carried out a rescue experiment, transforming the *atg1Δ:ATG1^{VE}-3 × GFP mCherry-ATG8* cells with plasmid-encoded unlabeled wild-type *ATG1*. This restored the formation of Atg8-labeled mature autophagosomes, but Atg1^{VE} remained punctate, confirming that the Atg1 AIM is necessary and sufficient for its localization to the growing phagophore (Figure 8B). When *atg1Δ:ATG1^{VE}-3 × GFP mCherry-ATG8* cells were rescued with plasmid-encoded kinase-dead *ATG1*, no mature autophagosomes were observed; when the rescue was done with plasmid-encoded *ATG1^{DD}*, a partial rescue was observed (Figure 8B).

DISCUSSION

Atg1 and Atg13 have well-characterized roles in autophagy initiation (Mizushima, 2010; Alers *et al.*, 2014; Noda and Fujioka, 2015; Lin and Hurley, 2016; Papinski and Kraft, 2016). Here, we report evidence for a function of Atg1 in autophagy distinct from its function in the initiating complex. Imaging of live cells showed a marked difference in localization of Atg1 and Atg13 relative to Atg8 marking the growing phagophore, supported by population-level analysis showing the expansion of the FWHM of the Atg1 signal only. Atg1 is often depicted as functioning within an obligate Atg1-Atg13-Atg17-Atg29-Atg31 complex throughout the course of autophagy. Quantitative (molecule-counting) microscopy shows that, averaged over the whole course of autophagy, Atg1 is twice as abundant as Atg13. SIM imaging showed that, in addition to its localization at the PAS, which it shares with Atg13, Atg1 is distinct from Atg13 in that it completely surrounds the mature autophagosome. These results are consistent with previous observations in an engineered version of the Cvt pathway expressing giant *Ape*I complexes (Suzuki *et al.*, 2013). These results also extend the implications of the studies that first identified the interaction between Atg1 and Atg8, which proposed that Atg1 remained associated with the autophagosome past the initiation stage (Kraft *et al.*, 2012; Nakatogawa *et al.*, 2012). Here, by using superresolution microscopy that can distinguish between different stages of autophagy, we show that Atg1 is indeed retained in later stages of autophagy and, importantly, that its behavior at this later stage is independent of binding Atg13.

The natural question following these observations is: What is the function of the Atg8- and AIM-dependent Atg1 association with the growing autophagosome? This stage is downstream of the best-understood functions of Atg1 in phosphorylating Atg9, which is upstream of Atg8 recruitment (Papinski *et al.*, 2014). It is also downstream of the putative activation of PI3K by Atg6 phosphorylation (Papinski and Kraft, 2016). We initially hypothesized that Atg might function in tethering small vesicles to contribute to phagophore expansion, given previous findings that the Atg1 EAT domain tethers small liposomes in vitro in the absence of Atg13 (Ragusa *et al.*, 2012). We identified a double-aspartate mutant, Atg1^{DD}, that shows wild-type binding to Atg13 by ITC, but a dramatic defect in bulk autophagy activity in vivo as measured by the Pho8Δ60 assay. *ATG1^{DD}* cells show somewhat reduced recruitment of Atg1^{DD} and Atg8 to the PAS, but the more dramatic effect is a complete block in phagophore expansion. This effect cannot be explained by a change in in vitro lipid tethering, however. These findings show that there is a critical function for Atg1-EAT that is independent of both its known Atg13-binding function and its speculative lipid-tethering function.

Some aspects of these observations may be pertinent to mammalian ULK1. The EAT domain structure of Atg1 and ULK1 is highly conserved, and many of the hydrophobic residues protruding from the EAT helices are conserved in ULK1. An ATG13-independent dominant-negative phenotype has been reported for kinase-dead ULK1 (Chan *et al.*, 2009). One difference is that ATG13 localizes to the growing phagophore in mammalian cells (Karanasios *et al.*, 2016), in contrast to yeast. ATG13 contains its own LIR (Alemu *et al.*, 2012),

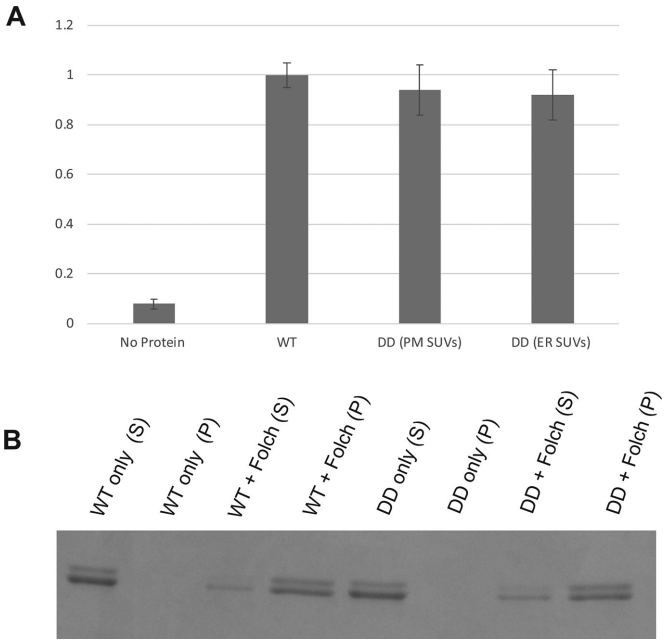

FIGURE 7: Vesicle tethering. (A) Sonicated small unilamellar vesicles containing either biotin or DID fluorescent label were mixed with either wild-type (WT) or DD mutant EAT domain. The mixture was then passed over streptavidin resin, capturing biotin-labeled vesicles, and the amount of fluorescently labeled vesicles was quantified. These data show that the DD mutation has no effect on the ability of the EAT domain to tether vesicles in vitro. (B) Liposome sedimentation assay of wild-type Atg1 and Atg1^{DD} incubated with Folch liposomes. Liposomes were ultracentrifuged at 50,000 rpm to separate supernatant and pellet fractions, and the presence of protein was analyzed by SDS–PAGE.

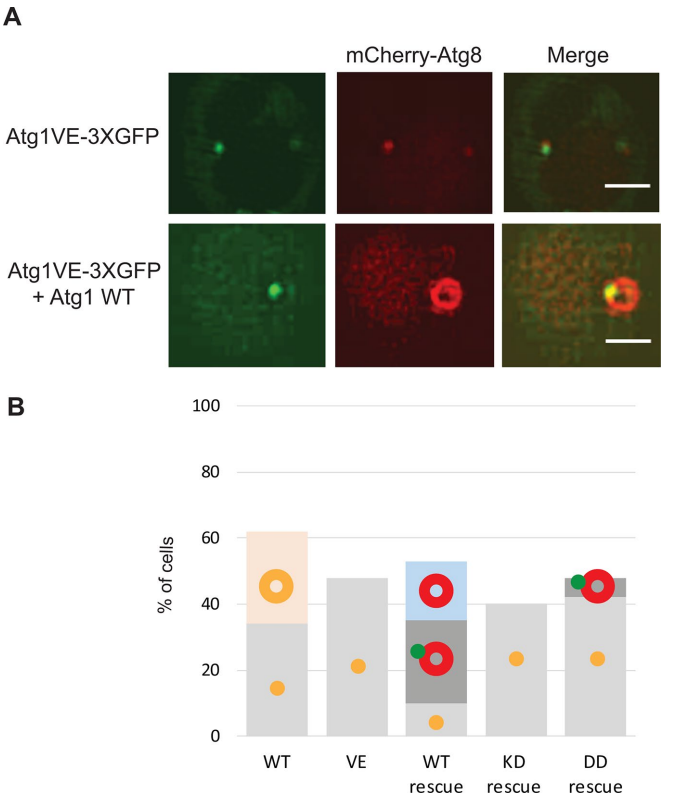

FIGURE 8: Atg1 interaction with Atg8 at the mature autophagosome. (A) SIM images of endogenous Atg1-VE mutant and mutant strain rescued with wild-type Atg1. Scale bar: 1 μm. (B) Quantitation of distribution of structures found in mutant and rescue cell lines. Quantitation of wild-type and rescue strains was done via SIM; quantitation of the VE mutant was done in wide-field microscopy after confirming the existence of only punctate structures via structured illumination. Wild type $n = 98$; wild-type (WT) rescue $n = 67$; VE mutant $n = 126$; kinase-dead (KD) rescue $n = 78$; DD rescue $n = 72$.

unlike yeast Atg13. Therefore, the apparent colocalization of ULK1 and ATG13 at the mammalian phagophore does not necessarily imply that all of this material is mutually exclusive of ULK1-independent function (Hieke *et al.*, 2015). Moreover, Atg8 is vital for autophagosome expansion in yeast (Xie *et al.*, 2008), while recent reports suggest that the cognate LC3/GABARAP family in mammals is much less important for expansion than had previously been supposed (Nguyen *et al.*, 2016; Tsuboyama *et al.*, 2016). LC3/GABARAP proteins in mammals are now proposed to be important mainly for selection of cargo and degradation of the inner autophagosomal membrane subsequent to autolysosome formation (Nguyen *et al.*, 2016; Tsuboyama *et al.*, 2016). In light of this new perspective, it is now unclear why Atg8 is so important for autophagosome expansion in yeast. Our results suggest that part of the explanation could be that Atg8 is essential for directing a late phase of some unidentified lipid- or protein-binding activity of Atg1 activity that is vital for associating with the source of incoming lipid for growth.

It is widely thought that IDRs and protein dynamics are a central feature of autophagy proteins. Yet techniques are lacking for directly measuring and controlling protein dynamics in living cells. As appealing as these concepts are, establishing the functional significance of disorder and dynamics in autophagy has been challenging, and only a handful of examples exist. Dynamic transitions from order to disorder have been shown to be relevant for BECN1 function in autophagy (Mei *et al.*, 2016). The Noda and Ohsumi groups were able to show that the yeast Atg13 IDR is important for the meshwork organization of the PAS (Yamamoto *et al.*, 2016). We previously showed that both the human PI3K complex I involved in autophagy induction and the yeast Atg1 EAT are dynamics entities (Baskaran *et al.*, 2014; Stjepanovic *et al.*, 2014). In the absence of Atg13, the Atg1 EAT domain and its helices 4 and 6, in particular, sample a highly dynamic "R" (relaxed state). Our engineered probe of the EAT domain includes a mutant located within helix 6 in this dynamic region. In addition to providing insight into an unappreciated facet of autophagosome expansion, our data add another example to the small but growing list of proteins with functionally essential dynamics in autophagy.

MATERIALS AND METHODS

Structured illumination microscopy

Atg1-3×EGFP pRS304-mcherry-Atg8 and *Atg13-3×EGFP pRS304-mcherry-Atg8* are derivatives of W303 (gifts from J. Nunnari, University of California, Davis) (Graef *et al.*, 2013). Endogenous Atg1 mutants were made by first replacing Atg1-3×EGFP with a NATMX6-selective cassette via PCR-based targeted homologous recombination. Using the *Atg1::NATMX6 pRS304-mcherry-Atg8* knockout strain, we then introduced the endogenous mutants via in vivo homologous recombination of PCR fragments containing the Atg1 mutation and the remainder of the cassette (3×EGFP-ADH terminator-CaURA). Positive recombinants were selected for on –ura plates and sequenced.

Yeast cells were grown overnight and then diluted to OD_{600} = ~0.2 the following morning in –trp media and grown for 4–5 h until OD_{600} = ~1.0. Meanwhile, coverglasses were cleaned via ultrasonication for 30 min in a 1:1 ratio of water and isopropanol, rinsed with water and isopropanol, and air-dried; coverglasses were then coated in 2 mg/ml concanavalin A.

One hour before imaging, 1 ml of yeast cells was treated with 0.2 µg/ml rapamycin to induce autophagy. For imaging, cells were placed on concanavalin A–coated coverslips and incubated for 15 min. Excess cells were washed off, and the coverglass was loaded onto an Attofluor chamber (Invitrogen); –trp media with 0.2 µg/ml rapamycin was added to the chamber to continue the autophagy-inducing treatment condition during imaging.

SIM was done using the Zeiss Elyra PS.1 with a 100× objective. GFP and mCherry signals were captured by lasers at 488 nm and 561 nm, respectively, used at 5% intensity and 100 ms exposure time. For each sample, *z* stacks were collected at 0.101 µm per slice, spanning 0.5 µm, and three 60° rotations were acquired.

For imaging wild-type Atg1 rescued strains, mutant strains were transformed with yCPLAC111-Atg1 and selected for on –leu plates. Transformants were restreaked and then grown overnight in –leu media. The next day, they were diluted to OD_{600} = 0.2 in –trp media, grown 4–5 h to OD_{600} = 1.0, and imaged as described above.

Tethering and sedimentation assays

Liposome-tethering assays were done with 3 µM protein and a total concentration of 2.5 mg/ml liposomes made by mixing mixing 1-palmitoyl-2-oleoyl-*sn*-glycero-3-phosphocholine (POPC), 1-palmitoyl-2-oleoyl-sn-glycero-3-phosphoethanolamine (POPE), L-α-phosphatidylinositol (POPI), 1-palmitoyl-2-oleoyl-*sn*-glycero-3-phospho-L-serine (POPS), and 1,2-dioleoyl-*sn*-glycero-3-phosphate (DOPA) dissolved in chloroform. DSPE-PEG2000-biotin and rhodamine-PE liposomes were made with 23.4% POPC, 20.3% POPE, 17.7% PI, 33.6% POPS, 3.9% DOPA, 0.1% rhodamine-PE, and 1% biotin-PE (Avanti Polar Lipids). DID (1,1′ dioctadecyl-3,3,3′,3′-tetramethylindodicarbocyanine) liposomes were made with 24.5% POPC, 20.3% POPE, 17.7% PI, 33.6% POPS, 3.9% DOPA, and 0.1% DID (Avanti Polar Lipids). For each sample, 50 µl of protein and 25 µl each of Biotin and DID liposomes were incubated with 50 µl preequilibrated MagStrep resin (Novagen) for 30 min and washed with buffer (20 mM Tris, pH 8, 200 mM NaCl). Liposomes and protein bound to resin were analyzed on SDS–PAGE, and the resulting gels were imaged with a Typhoon scanner. All samples were normalized to rhodamine fluorescence to account for the total amount of lipid bound to the resin.

For sedimentation assays, Folch fraction I (Sigma) lipids were dissolved in chloroform, vacuum-dried overnight, resuspended in 20 mM Tris, pH 8, 200 mM NaCl, and sonicated to form small unilamellar vesicles (SUVs). For each sample, 25 µl of 10 µM protein was mixed with 25 µl of 2.5 mg/ml liposomes (or buffer for the negative control). The mixture was incubated at room temperature for 30 min and then pelleted in an ultracentrifuge for 1 h at 50,000 rpm. Pellet and supernatant samples were collected, and the presence of protein was analyzed by SDS–PAGE.

Quantitative imaging of autophagy proteins

For quantitative imaging, the yeast strains *MATahis3Δ1 leu2Δ0 met15Δ0 ura3Δ0 ATG1-GFP*, *ATG13-GFP*, and *ATG17-GFP* were grown in yeast extract–peptone–dextrose (YPD) media supplemented with 2% glucose. For specifically studying macroautophagy, the cytoplasm-to-vacuole transport protein Atg11 was knocked out and replaced by an NATMX cassette. The strain JBY404, expressing dimeric LacO-binding protein LacI-GFP binding to 128 *LacO* repeats, was used as a standard.

Yeast cells were grown overnight and then diluted to OD_{600} = ~0.2 the following morning in –trp media and grown for 4–5 h to OD_{600} = ~1.0. Meanwhile, coverglasses were cleaned via ultrasonication for 30 min in a 1:1 ratio of water and isopropanol, rinsed with water and isopropanol, and air-dried; coverglasses were then coated in 2 mg/ml concanavalin A.

One hour before imaging, yeast cells (1 ml) were treated with 0.2 µg/ml rapamycin to induce autophagy. For imaging, cells were placed on concanavalin A–coated coverslips and incubated for 15 min. Excess cells were washed off, and the coverglass was loaded onto an Attofluor chamber (Invitrogen); –trp media with 0.2 µg/ml rapamycin was added to the chamber to continue the autophagy-inducing treatment condition during imaging.

Wide-field fluorescence imaging was done on a Nikon Ti-E-based microscope with a 100× TIRF 1.49 NA oil objective.

Yeast autophagy assays

TN124 *Atg1*::NATMX cells were transformed with yCPLAC33, *ATG1*-yCPLAC33, *ATG1^{VE}*-yCPLAC33, or *ATG1^{DD}*-yCPLAC33 and grown to mid–log phase. Cells were then switched to nitrogen-starvation media for 4 h to induce autophagy, and the Pho8Δ60 assay was carried out as previously described (Klionsky, 2007).

For mCherry-Atg8–processing assays, *ATG1-3 × GFP mCherry-ATG8* cells, *ATG13-3 × GFP mCherry-ATG8*, and endogenous *ATG1* mutant cells were grown to mid–log phase and then switched to nitrogen-starvation media for 4 h to induce autophagy. Cells were lysed and processed, and mCherry was detected by Western blot (anti-RFP, Rockland, 600-401-379).

Western blotting

For quantifying the expression levels of Atg1 constructs, TN124 *Atg1*::NATMX was first transformed with *ATG1-GFP* (wild type or mutants) subcloned into pJK59. Overnight cultures were split to OD_{600} = 0.2 and grown to OD_{600} = 0.9 in –ura medium; 45 ml of yeast cells was harvested. The pellet was resuspended in 220 µl of 50 mM Tris (pH 8.0), 1% SDS, 7 M urea,1 mM EDTA, and 2 mM phenylmethylsulfonyl fluoride; lysed in 0.13 g of 425–600 mm glass beads (Sigma G8772); and vortexed vigorously for 4 min at 4°C. Cell lysates were subjected to Western blot analysis using a mouse anti-GFP antibody (Santa Cruz sc9996) at a 1:1000 ratio, anti-mouse immunoglobulin G–horseradish peroxidase (PerkinElmer NEF822001EA) at a 1:5000 ratio, and Pierce ECL Western blotting substrate (Thermo Scientific 32209). Antibody to PGK1 (Invitrogen 459250) was used as a loading control.

Immunoprecipitation

For quantifying the interaction of wild-type Atg1 and Atg1^{DD} with Atg8 and Atg13, sequences encoding *S. cerevisiae* Atg8 and *S. cerevisiae* Atg13$_{432–520}$, encompassing the Atg1-binding region, were cloned into vector pGST2. These constructs were then expressed, and GST-Atg8 and GST-Atg13 were purified from *Escherichia coli*. For the immunoprecipitation experiment, *ATG1-3 × GFP mCherry-ATG8* and *ATG1^{DD}-3 × GFP mCherry-ATG8* cells were grown to mid–log phase and switched to nitrogen-starvation media for 4 h to induce autophagy. The cell lysate was incubated with GFP-Trap beads (Chromotek) for 1 h at 4°C. After washing, 2 µM of GST-Atg8 or GST-Atg13 was added, and the mixture was incubated for 1 h at 4°C. The beads were then washed (10 mM Tris, pH 7.5, 450 mM NaCl, 5 mM $MgCl_2$) and boiled in 2× SDS for 5 min, and the presence of protein was

analyzed via Western blot (anti-GST, sc-459). PGK1 was used as a loading control.

Isothermal titration calorimetry

Proteins were dialyzed in 20 mM Tris-HCl (pH 8.0) and 200 mM NaCl, with 1 mM Tris(2-carboxyethyl)phosphine added for Atg1-EAT. ITC was conducted with a MicroCal Auto-iTC200 apparatus (GE Healthcare) at 20°C with 20 total injections of 2 µl per injection. The binding affinity between *K. lactis* Atg13 350-525 and Atg1-EAT was determined by using 10 µM maltose-binding protein (MBP)-tagged Atg13 350-525 in the cell and 100 µM Atg1-EAT in the syringe. MBP alone plus Atg1-EAT was used as a control.

Image processing and analysis

Image processing consisted of the following steps. The inputs for image processing were wide-field microscopy image stacks that show, on average, ~300 cells on a 2560 × 2160 pixel (166 × 140 µm) field of view in ~50 frames, recorded at 10 fps for a total observation time of ~8 min. For each labeled species, candidate puncta were identified by using the Fiji (Schindelin *et al.*, 2012) plug-in TrackMate v. 2.8.2 (Tinevez *et al.*, 2017) with a Laplacian of Gaussian detection for the average puncta size of ~12–15 pixels. TrackMate was then used to filter the list of candidates by tracking the puncta and retaining only those that persisted for at least five consecutive frames. This initial list of puncta candidates was exported as an XML file for further processing. A custom-written Python v. 2.7.12 code was used to match found puncta traces from labeled conditions with one another to further refine the list of puncta (i.e., a trace was accepted if both labeled species could be identified on a PAS for at least five consecutive frames). For this list of puncta, custom-made Python v. 2.7.12 and iPython v. 4.0.1 scripts were used to subtract the background and to fit a two-dimensional Gaussian to the microscopy intensity at every time point in each trace. The reference species Atg8 was used to align the fitted two-dimensional Gaussians for each trace. The peak intensity of Atg8 was chosen as the alignment time point. From the aligned traces, the average punctum intensity and width over time were extracted by calculating the FWHM of the fitted Gaussian at each time point.

ACKNOWLEDGMENTS

We thank members of the Hurley, Drubin, Rine, Koshland, and Thorner labs for discussions and advice and J. Nunnari for yeast strains. SIM was carried out at the CNR Biological Imaging Facility at the University of California, Berkeley (National Institutes of Health grant 1S10OD018136-01). This work was supported by National Institutes of Health grant GM111730 (to J.H.H.) and Ruth Kirschstein National Research Service Award GM112301 (to C.W.D.).

REFERENCES

Alemu EA, Lamark T, Torgersen KM, Birgisdottir AB, Larsen KB, Jain A, Olsvik H, Øvervatn A, Kirkin V, Johansen T (2012). ATG8 family proteins act as scaffolds for assembly of the ULK complex: sequence requirements for LC3-interacting region (LIR) motifs. J Biol Chem 287, 39275–39290.

Alers S, Wesselborg S, Stork B (2014). ATG13. Autophagy 10, 944–956.

Baskaran S, Carlson L-A, Stjepanovic G, Young LN, Kim DJ, Grob P, Stanley RE, Nogales E, Hurley JH (2014). Architecture and dynamics of the autophagic phosphatidylinositol 3-kinase complex. eLife 3, https://doi.org/10.7554/eLife.05115.

Bento CF, Renna M, Ghislat G, Puri C, Ashkenazi A, Vicinanza M, Menzies FM, Rubinsztein DC (2016). Mammalian autophagy: how does it work? Annu Rev Biochem 85, 685–713.

Brickner JH, Walter P, Strohmann B, Schuller H, Weissman J (2004). Gene recruitment of the activated INO1 locus to the nuclear membrane. PLoS Biol 2, e342.

Chan EYW, Longatti A, McKnight NC, Tooze SA (2009). Kinase-inactivated ULK proteins inhibit autophagy via their conserved C-terminal domains using an Atg13-independent mechanism. Mol Cell Biol 29, 157–171.

Cheong H, Yorimitsu T, Reggiori F, Legakis JE, Wang C-W, Klionsky DJ (2005). Atg17 regulates the magnitude of the autophagic response. Mol Biol Cell 16, 3438–3453.

Fujioka Y, Suzuki SW, Yamamoto H, Kondo-Kakuta C, Kimura Y, Hirano H, Akada R, Inagaki F, Ohsumi YNN (2014). Structural basis of starvation-induced assembly of the autophagy initiation complex. Nat Struct Mol Biol 21, 513–521.

Funakoshi T, Matsuura A, Noda T, Ohsumi Y (1997). Analyses of APG13 gene involved in autophagy in yeast, *Saccharomyces cerevisiae*. Gene 192, 207–213.

Geng J, Baba M, Nair U, Klionsky DJ (2008). Quantitative analysis of autophagy-related protein stoichiometry by fluorescence microscopy. J Cell Biol 182, 129–140.

Graef M, Friedman JR, Graham C, Babu M, Nunnari J (2013). ER exit sites are physical and functional core autophagosome biogenesis components. Mol Biol Cell 24, 2918–2931.

Hieke N, Löffler AS, Kaizuka T, Berleth N, Böhler P, Drießen S, Stuhldreier F, Friesen O, Assani K, Schmitz K, *et al.* (2015). Expression of a ULK1/2 binding-deficient ATG13 variant can partially restore autophagic activity in ATG13-deficient cells. Autophagy 11, 1471–1483.

Hurley JH, Young LN (2017). Mechanisms of autophagy initiation. Annu Rev Biochem 86, 225–244.

Jao CC, Ragusa MJ, Stanley RE, Hurley JH (2013). A HORMA domain in Atg13 mediates PI 3-kinase recruitment in autophagy. Proc Natl Acad Sci USA 110, 5486–5491.

Kabeya Y, Kamada Y, Baba M, Takikawa H, Sasaki M, Ohsumi Y (2005). Atg17 functions in cooperation with Atg1 and Atg13 in yeast autophagy. Mol Biol Cell 16, 2544–2553.

Kamada Y, Yoshino K, Kondo C, Kawamata T, Oshiro N, Yonezawa K, Ohsumi Y (2010). Tor directly controls the Atg1 kinase complex to regulate autophagy. Mol Cell Biol 30, 1049–1058.

Karanasios E, Walker SA, Okkenhaug H, Manifava M, Hummel E, Zimmermann H, Ahmed Q, Domart MC, Collinson L, Ktistakis NT (2016). Autophagy initiation by ULK complex assembly on ER tubulovesicular regions marked by ATG9 vesicles. Nat Commun 7, 12420.

Klionsky DJ (2007). Monitoring autophagy in yeast: the Pho8Delta60 assay. Methods Mol Biol 390, 363–371.

Klionsky DJ, Schulman BA (2014). Dynamic regulation of macroautophagy by distinctive ubiquitin-like proteins. Nat Struct Mol Biol 21, 336–345.

Köfinger J, Ragusa MJ, Lee I-H, Hummer G, Hurley JH (2015). Solution structure of the Atg1 complex: implications for the architecture of the phagophore assembly site. Structure 23, 809–818.

Kraft C, Kijanska M, Kalie E, Siergiejuk E, Lee SS, Semplicio G, Stoffel I, Brezovich A, Verma M, Hansmann I, *et al.* (2012). Binding of the Atg1/ULK1 kinase to the ubiquitin-like protein Atg8 regulates autophagy. EMBO J 31, 3691–3703.

Lin MG, Hurley JH (2016). Structure and function of the ULK1 complex in autophagy. Curr Opin Cell Biol 39, 61–68.

Mari M, Griffith J, Rieter E, Krishnappa L, Klionsky D, Reggiori F (2010). An Atg9-containing compartment that functions in the early steps of autophagosome biogenesis. J Cell Sci 190, 1005–1022.

Mei Y, Glover K, Su M, Sinha SC (2016). Conformational flexibility of BECN1: essential to its key role in autophagy and beyond. Protein Sci 25, 1767–1785.

Mizushima N (2007). Autophagy: process and function. Genes Dev 21, 2861–2873.

Mizushima N (2010). The role of the Atg1/ULK1 complex in autophagy regulation. Curr Opin Cell Biol 22, 132–139.

Mizushima N, Komatsu M (2011). Autophagy: renovation of cells and tissues. Cell 147, 728–741.

Mizushima N, Levine B, Cuervo AM, Klionsky DJ (2008). Autophagy fights disease through cellular self-digestion. Nature 451, 1069–1075.

Mizushima N, Yoshimori T, Ohsumi Y (2011). The role of Atg proteins in autophagosome formation. Annu Rev Cell Dev Biol 27, 107–132.

Nakatogawa H, Ohbayashi S, Sakoh-Nakatogawa M, Kakuta S, Suzuki SW, Kirisako H, Kondo-Kakuta C, Noda NN, Yamamoto H, Ohsumi Y (2012). The autophagy-related protein kinase Atg1 interacts with the ubiquitin-like protein Atg8 via the Atg8 family interacting motif to facilitate autophagosome formation. J Biol Chem 287, 28503–28507.

Nakatogawa H, Suzuki K, Kamada Y, Ohsumi Y (2009). Dynamics and diversity in autophagy mechanisms: lessons from yeast. Nat Rev Mol Cell Biol 10, 458–467.
Nguyen TN, Padman BS, Usher J, Oorschot V, Ramm G, Lazarou M (2016). Atg8 family LC3/GABARAP proteins are crucial for autophagosome–lysosome fusion but not autophagosome formation during PINK1/Parkin mitophagy and starvation. J Cell Biol 215, 857–874.
Noda NN, Fujioka Y (2015). Atg1 family kinases in autophagy initiation. Cell Mol Life Sci 72, 3083–3096.
Papinski D, Kraft C (2016). Regulation of autophagy by signaling through the Atg1/ULK1 complex. J Mol Biol 428, 1725–1741.
Papinski D, Schuschnig M, Reiter W, Wilhelm L, Barnes CA, Maiolica A, Hansmann I, Pfaffenwimmer T, Kijanska M, Stoffel I, *et al.* (2014). Early steps in autophagy depend on direct phosphorylation of Atg9 by the Atg1 kinase. Mol Cell 53, 471–483.
Popelka H, Uversky VN, Klionsky DJ (2014). Identification of Atg3 as an intrinsically disordered polypeptide yields insights into the molecular dynamics of autophagy-related proteins in yeast. Autophagy 10, 1093–1104.
Ragusa MJ, Stanley RE, Hurley J (2012). Architecture of the Atg17 complex as a scaffold for autophagosome biogenesis. Cell 151, 1501–1512.
Reggiori F, Klionsky DJ (2013). Autophagic processes in yeast: mechanism, machinery and regulation. Genetics 194, 341–361.
Schindelin J, Arganda-Carreras I, Frise E, Kaynig V, Longair M, Pietzsch T, Preibisch S, Rueden C, Saalfeld S, Schmid B, *et al.* (2012). Fiji: an open-source platform for biological-image analysis. Nat Methods 9, 676–682.
Stjepanovic G, Davies CW, Stanley RE, Ragusa MJ, Kim DJ, Hurley JH (2014). Assembly and dynamics of the autophagy-initiating Atg1 complex. Proc Natl Acad Sci USA 111, 12793–12798.
Suzuki K, Akioka M, Kondo-Kakuta C, Yamamoto H, Ohsumi Y (2013). Fine mapping of autophagy-related proteins during autophagosome formation in *Saccharomyces cerevisiae*. J Cell Sci 126, 2534–2544.
Suzuki K, Kubota Y, Sekito TOY (2007). Hierarchy of Atg proteins in pre-autophagosomal structure organization. Genes Cells 12, 209–218.
Teis D, Saksena S, Emr SD (2008). Ordered assembly of the ESCRT-III complex on endosomes is required to sequester cargo during MVB formation. Dev Cell 15, 578–589.
Tinevez J-Y, Perry N, Schindelin J, Hoopes GM, Reynolds GD, Laplantine E, Bednarek SY, Shorte SL, Eliceiri KW (2017). TrackMate: an open and extensible platform for single-particle tracking. Methods 115, 80–90.
Tsuboyama K, Koyama-Honda I, Sakamaki Y, Koike M, Morishita H, Mizushima N (2016). The ATG conjugation systems are important for degradation of the inner autophagosomal membrane. Science 354, 1036–1041.
Wen X, Klionsky DJ (2016). An overview of macroautophagy in yeast. J Mol Biol 428, 1681–1699.
Xie Z, Nair U, Klionsky DJ (2008). Atg8 controls phagophore expansion during autophagosome formation. Mol Biol Cell 19, 3290–3298.
Yamamoto H, Fujioka Y, Suzuki SW, Noshiro D, Suzuki H, Kondo-Kakuta C, Kimura Y, Hirano H, Ando T, Noda NN, *et al.* (2016). The intrinsically disordered protein Atg13 mediates supramolecular assembly of autophagy initiation complexes. Dev Cell 38, 86–99.
Yamamoto H, Kakuta S, Watanabe TM, Kitamura A, Sekito T, Kondo-Kakuta C, Ichikawa R, Kinjo M, Ohsumi Y (2012). Atg9 vesicles are an important membrane source during early steps of autophagosome formation. J Cell Biol 198, 219–233.
Yan J, Kuroyanagi H, Kuroiwa A, Matsuda Y, Tokumitsu H, Tomoda T, Shirasawa T, Muramatsu M (1998). Identification of mouse ULK1, a novel protein kinase structurally related to *C. elegans* UNC-51. Biochem Biophys Res Commun 246, 222–227.
Yeh Y-Y, Shah KH, Herman PK (2011). An Atg13 protein-mediated self-association of the Atg1 protein kinase is important for the induction of autophagy. J Biol Chem 286, 28931–28939.
Yorimitsu T, Klionsky DJ (2005). Atg11 links cargo to the vesicle-forming machinery in the cytoplasm to vacuole targeting pathway. Mol Biol Cell 16, 1593–1605.